*Int. J. Electrochem. Sci.*, 10 **(2015)** 6959 - 6974

International Journal of
ELECTROCHEMICAL
SCIENCE
www.electrochemsci.org

# Organic Clathrate Compounds as Suitable Transducers in Electrochemical Sensing

*Kanyisa L Nohako*[*], *Priscilla GL Baker, Emmanuel I Iwuoha*

SensorLab, Chemistry department, University of the Western Cape, Private Bag X17, Bellville7535
[*]E-mail: knohako@yahoo.com

*Received:* 15 May 2015 / *Accepted:* 13 July 2015 / *Published:* 28 July 2015

We have successfully synthesised 9,9'-(ethyne1,2-diyl)bis(flouren-9-ol) by reflux method and 9-(4-methoxyphenyl)-9H-xanthen-9-ol through stirring at room temperature. The products were characterised using spectroscopic methods and were found to be both UV/vis active ($\lambda_{max}$ = 400 nm flourene derivative and $\lambda_{max}$ = 337 nm xanthene derivative) and fluorescent (440nm and 467nm flourene derivative and 344 and 380 xanthene derivative). These compounds were drop coated onto commercial glassy carbon electrode (GCE) to produce thin films. Scan rate dependent cyclic voltammetry (CV) confirmed the electrodynamics of the thin films to be consistent with monolayer diffusion ($D_e$ = 8.91x10$^{-6}$cm$^2$s$^{-1}$ flourene derivative and $D_e$ = 1.05x10$^{-10}$cm$^2$s$^{-1}$ xanthene derivative). Surface concentration was estimated to be 1.55x10$^{-13}$ mol cm$^{-2}$ flourene derivative and 2.00x10$^{-13}$ mol cm$^{-2}$. Electrochemical impedance confirmed the electroactivity of the materials as indicated by very low interfacial capacitance and low charge transfer resistance values.

**Keywords:** Clathrate, voltammetry, differential scanning calorimeter, powder x-ray diffraction, fluorescence.

## 1. INTRODUCTION

In supramolecular chemistry clathrates are a fundamental topic due to their great promise in a variety of practical matters such as the separation of small molecules on the basis of size exclusion or chemical affinity, the potential to accommodate guest molecules with desirable optical properties and to be utilized in chemical sensor development[1].

Cyclodextrin clathrates are widely used due to their structural characteristics and special functions[2]. They are cyclic oligosaccharides comprising of glucopyranose units linked by α-(1,4) bonds soluble in water [3; 4]. α-, β-, γ-cyclodextrins are commonly available and have a donut shaped cavity with internal cavity diameters of 4.2, 7.8 and 9.5 Å [3] respectively. β-cyclodextrin is perhaps

most widely used, since it is readily available from chemical suppliers. [4]. The cyclodextrin clathrates can form host – guest complexes with many compounds in the gas, aqueous or solid state by inclusion phenomena based on lock and key model. The model employs a host molecule (lock) that is able to entrap a highly selective target molecule (key) either permanently or temporarily. These types of systems are efficient recognition partners in sensing systems and various other applications [4]. An electrochemical sensor designed by Fang et.al., proved highly successful in the voltammetric detection of organic compounds at a higly ordered self-assembled lipoyl-β-cyclodextrin derivate monolayer on gold electrode. This sensor convincingly demonstrated the host-guest capability of clathrate compounds coupled to electrochemical analysis as an effective analytical protocol for the detection of electro inactive organic species [2]. Organic polymers with regularly repeating and highly conjugated units in their backbone such as polypyrrole, polyaniline, polythiophenes and polyphenylene vinylenes have been used as semi-conductive platforms in many electrochemical sensor applications. Their unique optical and electrical properties are due to π-electrons delocalized over the regularly repeating units in the backbone of the polymer[5]. They can be obtained chemically or electrochemically from their equivalent monomers. Here we report for the first time the characterization of 9,9'-(ethyne1,2-diyl)bis(flouren-9-ol) and 9-(4-methoxyphenyl)-9H-xanthen-9-ol using differential scanning calorimeter, infrared spectroscopy, ultraviolet visible spectroscopy, flourescence spectroscopy and their electrochemistry using cyclic voltammetry, squarewave voltammetry and electrochemical impedance spectroscopy. Flourene derivative and xanthene derivative are both rigid and bulky conforms to Weber's host design rule[1]. They are porous noncyclic compounds with highly hydrophobic surface.

## 2. EXPERIMENTAL PROCEDURES

### *2.1. Reagents*

Sulphuric acid, ethylmagnesium bromide, flourenone, ammonium chloride, n-hexane anhydrous sodium sulphate, magnesium turnings xanthone and magnesium sulphate were purchased from Merck. Tetrahydrofuran and anisole were purchased from Sigma-Aldrich. Phosphate buffer, 0.2 M, pH 7.12 was prepared from anhydrous disodium hydrogen phosphate and sodium dihydrogen phosphate. All these chemicals were of analytical grade. Deionized water purified by milli-QTM system was utilized for aqueous solution preparations. Analytical grade Argon supplied by Afrox South Africa was used to degas the system.

### *2.2. Apparatus and electrode preparation*

#### *2.2.1. Apparatus*

Characterization was done using Differential scanning calorimeter (DSC) Perkin Elmer DSC6000, Fourier transform infrared (FTIR) Perkin Elmer Spectrum 100, Ultra violet visible spectra

were measured using Nicolette Evolution 100 Spectrometer (Thermo Electron Corporation, UK) and pH meter. Electrochemical experiments were performed using BAS100W Bioanalytical System (Model No. 100B). The three electrode cell composed of a platinum wire as counter electrode, a Ag/AgCl (3 M) reference electrode and glassy carbon working electrode. Powder X-ray diffraction (BRUKER D8-ADVANCE diffractometer CuKα1 1.54 Å) and Fluorescence spectroscopy, was used for further characterization.

*2.3. Synthesis of organic clathrates*

Organic clathrates were synthesized using Grignard reagents. The Grignard reagent used in the preparation of 9-(4-methoxyphenyl)-9H-xanthen-9-ol was prepared fresh in our laboratories, following the method detailed below:

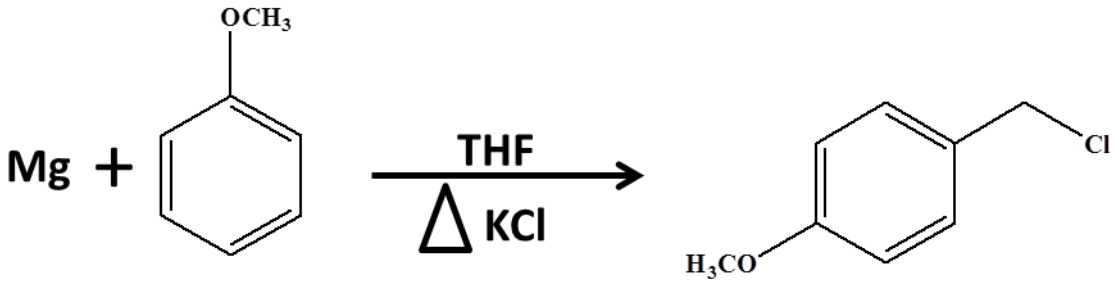


**Scheme 1.** Grignard reagent preparation

*2.3.1. 9,9'-(ethyne1,2-diyl)bis(flouren-9-ol) (Flourene derivative) synthesis*

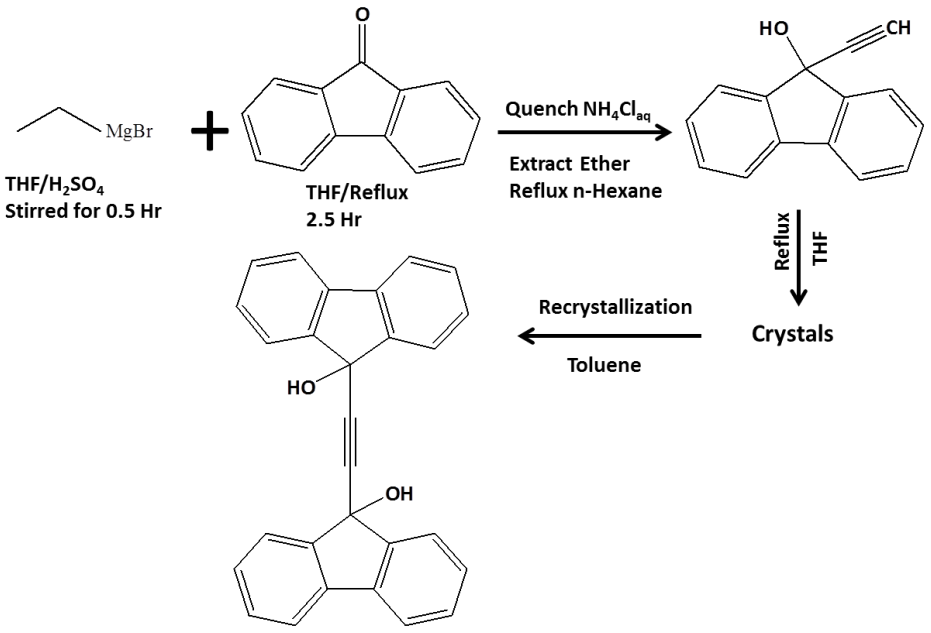


**Scheme 2.** Flourene derivative synthesis.

A solution of ethylmagnesium bromide (150 ml) was added to dry THF (200ml) saturated with concentrated sulphuric acid. The mixture was stirred for 0.5hour. A solution of flourenone (0.36 mol) in dry THF (300 ml) was added. The mixture was heated to reflux for 2 hours then cooled and quenched with saturated aqueous ammonium chloride solution. The ethereal phase was separated and the aqueous phase was extracted with diethyl ether. The combined organic phases were dried (anhydrous sodium sulphate) and the solvents were evaporated. The oily residue was extracted with refluxing *n*-hexane, the residue that did not dissolve in *n*-hexane was extracted with refluxing THF and cooled to give crystals of the clathrate. Recrystallization from toluene yielded 2g of yellow powder [1].

*2.3.2. 9-(4-methoxyphenyl)-9H-xanthen-9-ol (Xanthene derivative) synthesis*

Grignard reagent was prepared under nitrogen from 9g of magnesium turnings and 29 ml of anisole in 100 ml of dry THF. A small crystal of iodine and warming of the reaction mixture was required to initiate the reaction. The mixture was refluxed for 2.5 hours after addition of halide solution (potassium chloride) was complete. The Grignard reagent was transferred by syringe to the addition funnel on a dried nitrogen filled flask containing 75 ml of dry THF and 19.6g of xanthone. The Grignard solution was added rapidly dropwise to the ketone. The suspension formed was diluted with an additional 50 m of dry THF and stirred at room temperature for 7 hours. It was then quenched with aqueous ammonium chloride and extracted with ether. The ethereal phase was washed, dried (magnesium sulphate) and condensed to yield 3.5g of white powder [6].

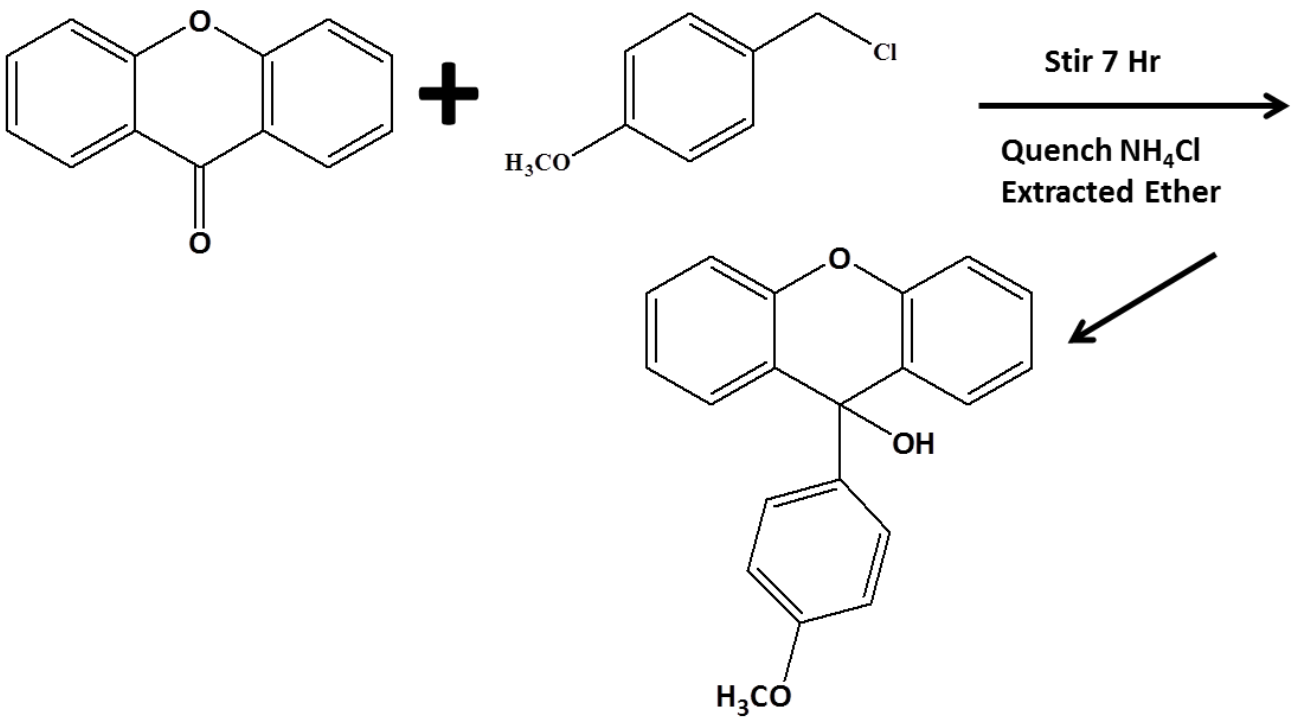


**Scheme 3.** Xanthene derivative synthesis.

### *2.4. Sample preparation*

#### *2.4.1. Differential Scanning Calorimeter (DSC)*

The experimental traces were recorded at a heating rate of 10 K min-1 and under an inert atmosphere of nitrogen gas with a flow rate of 20 cm3 min-1. The samples were used as they are (powder). The sample masses ranged between 2-4 mg. This method uses two identical 50 μL crimped and vented aluminium pans, one contains a sample and the other is empty and used as a reference.

#### *2.4.2. Fourier transform infrared spectroscopy (FTIR)*

The sample holder was cleaned using acetone, the sample was then transferred onto the sample holder and it was pressed, then the spectrum was recorded.

#### *2.4.3. Ultraviolet visible spectroscopy (UV-vis) and Fluorescence spectroscopy*

Analysis was performed by dissolving flourene derivative in methanol and xanthene derivative in ethanol for both instruments. A yellow solution was observed for both clathrates.

#### *2.4.4. Powder X-ray diffraction (PXRD)*

Powdered samples were placed on X-ray insensitive Mylar film. The intensities of the diffraction spots were measured using BRUKER D8-ADVANCE diffractometer CuKα1 (1.54 Å) radiation produced at 40 kV and 40 mA. PXRD experiments were completed at iThemba labs.

#### *2.4.5. Cyclic voltammetry (CV) and Square wave voltammetry (SWV)*

The preparation was the same for CV and SWV analysis. A layer of each clathrate compound was deposited by drop-coating on the glassy carbon electrode and the electroactivity was evaluated. The measurements were carried out in pH 7.12, 0.2 M phosphate buffer at the potential window; -700 mV to 800 mV for flourene derivative and -1000mV to 1000 mV for xanthene derivative at scan rates of 20, 40, 60, 80 and 100 mVs-1 for CV and at scan rates of 75, 150 and 300 mVs-1 for SWV.

#### *2.4.6. Electrocemical impedance spectroscopy (EIS)*

EIS measurements were carried out in 0.2 M pH 7.12 PBS at a fixed potential of -134 mV for flourene derivative and -73.5 mV for xanthene derivative where clathrate platforms interfacial parameters were investigated.

*2.5. Electrode preparation*

Working electrode (glassy carbon electrode GCE) was polished using 1µ, 0.3µ and 0.05µ alumina powder. After each polishing the electrode was rinsed with distilled water. It was then sonicated in ethanol and in water and finally air dried.

## 3. RESULTS AND DISCUSSION

*3.1. Differential Scanning Calorimeter*

We investigated the thermal profile of the powder synthesized by DSC. Flourene derivative yielded a single broad endotherm corresponding to its melting point of 221 °C (fig 1A). Weber and co-workers [1] has found the melting point to be in the range of 244 - 245 °C. Figure 1B reveals two endotherms, first endotherm is due to the melting point of xanthene derivative at 176 °C and the second endotherm is due to the decomposition of the compound.

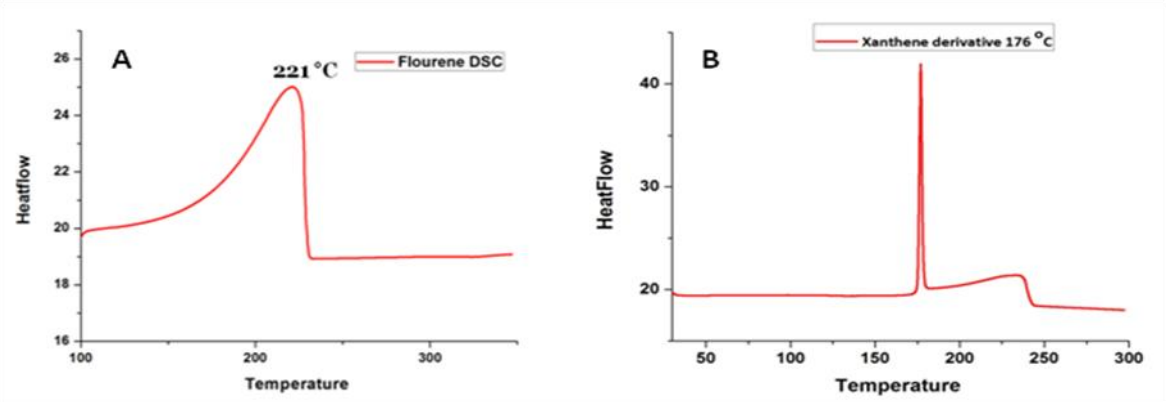


**Figure 1.** A) DSC curve showing melting point of flourene derivative. B) DSC curve showing melting point of xanthene derivative.

*3.2. Fourier transform infrared spectroscopy*

FTIR spectra of the flourene derivative and xanthene derivative compounds supported their structure. Fig 2A shows characteristics absorption bands around 3200 $cm^{-1}$ due to O-H stretching, 2169 $cm^{-1}$ due to C≡C stretching, around 1603-1447 $cm^{-1}$ due to C=C aromatic stretch and around 1149-922 $cm^{-1}$ corresponding to C-O stretch from alcohol. Xanthene derivative exhibited characteristics absorption bands around 3750 $cm^{-1}$ corresponding to O-H stretch, around 2669 $cm^{-1}$ due to C-H stretch from aromatic ring, around 1656-1447 $cm^{-1}$ due to C=C stretch aromatics and around 1339-1147 $cm^{-1}$ corresponding to C-O-C stretch. A Xathene derivative spectrum was compared with the xanthone spectra (starting material) and it was concluded that a new compound was synthesized (fig 2B).

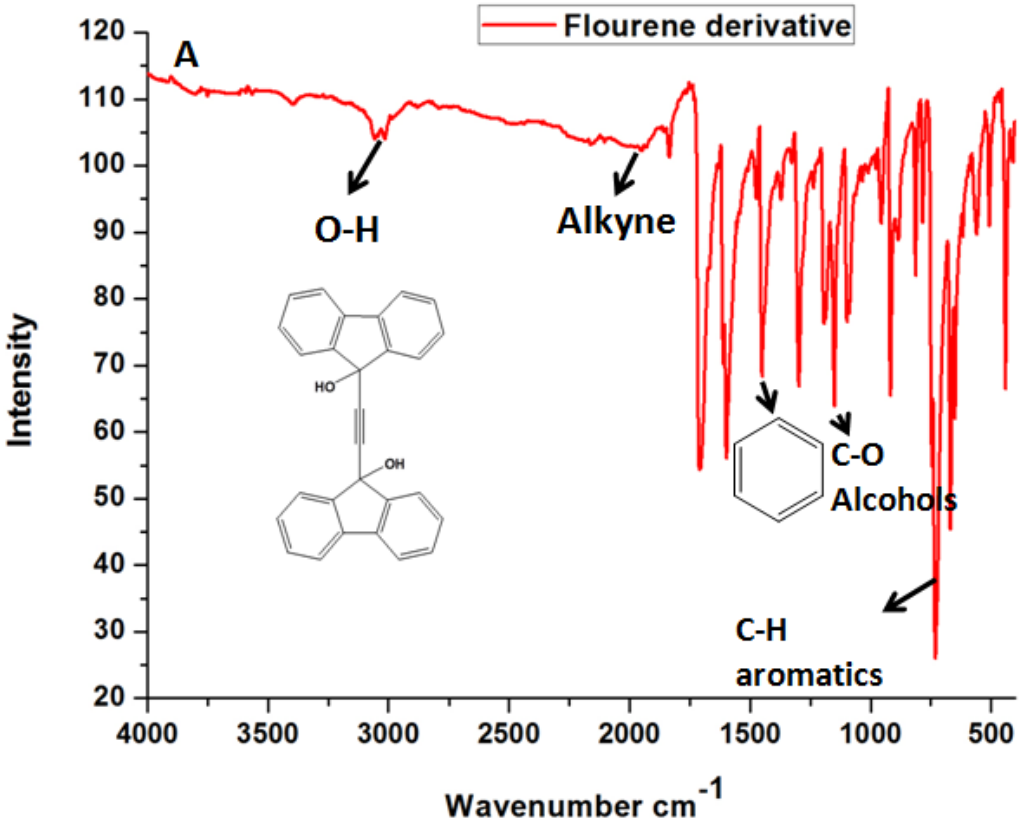


**Figure 2(a).** IR spectrum showing flourene derivative functional groups.

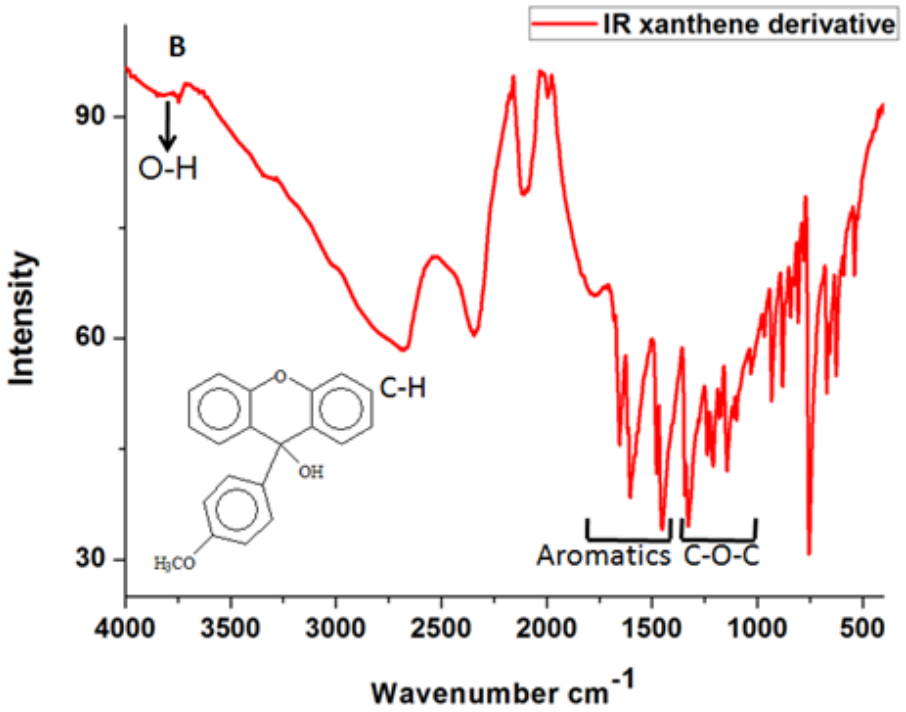


**Figure 2(b).** IR spectrum showing functional groups of xanthene derivative

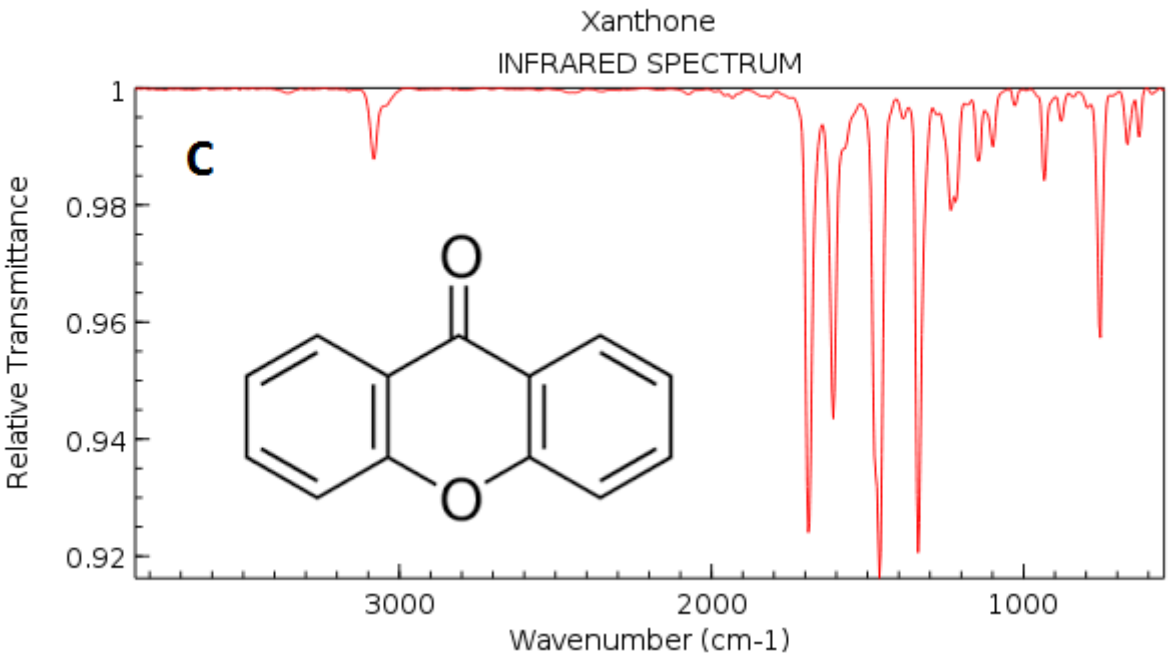


**Figure 2(c).** Spectra for xanthone starting material.

*3.3. Ultraviolet visible spectroscopy*

UV/Vis was performed to determine the energy gap for both clathrates. For flourene derivative, fig 3A shows a broad peak with absorption maxima of 400 nm which is attributed to the $\pi$-$\pi^*$ transition with the band gap of 3.1 eV. The band gap was calculated using the formula

$$EG = {}^{1240}/_{\lambda}$$ Equation (1) [7].

Similar absorption spectra was observed for difluorene substituted carbazole (DFC) [8] and poly[2,7'-(ethyl 9,9-dioctyl-7,2'-biflourene-9-carboxylate)] [9]. For xanthene derivative absorption spectra (fig 3B) showed a narrow peak with a little shoulder and the absorption maxima of 337 nm due to $\pi$-$\pi^*$ transition with energy gap of 3.6 eV calculated using equation 1. Rhodamine B also showed similar absorption spectra with the maxima of 555 nm. Xanthenes form aggregates that modify the absorption spectrum and photophysical properties that affect the ability to emit. Band splitting is always observed for the xanthenes indicating that these aggregates are neither parallel nor linear but have intermediate geometry [10]. Flourene-substituted pyrenes have been reported to improve transporting ability in organic light emitting diodes (OLEDs) due to their high energy levels of the HOMO (-5.2 eV) with energy gap of 3.05 eV. Pyrene derivatives are widely used as probe in recognizing DNA labels because of their strong $\pi$ electron delocalization energy and efficient fluorescence properties due to the large planar conjugated aromatic characteristic [11]. These derivates are used as guests in phosphorescent emitters, they increase the efficiency of the light emitting diodes [12]. Compounds that are less conjugated have a bigger band gap and that results in the decrease in

conductivity [13]. Natural polyaniline was reported to have a band gap of 2.8 eV[14] and strong absorption for visible light, tungsten oxide was also reported to have a band gap of 2.8 eV[15]. For all materials i.e. clathrates, polymers and metal oxides the values obtained for band gap are within the range of semiconductors.

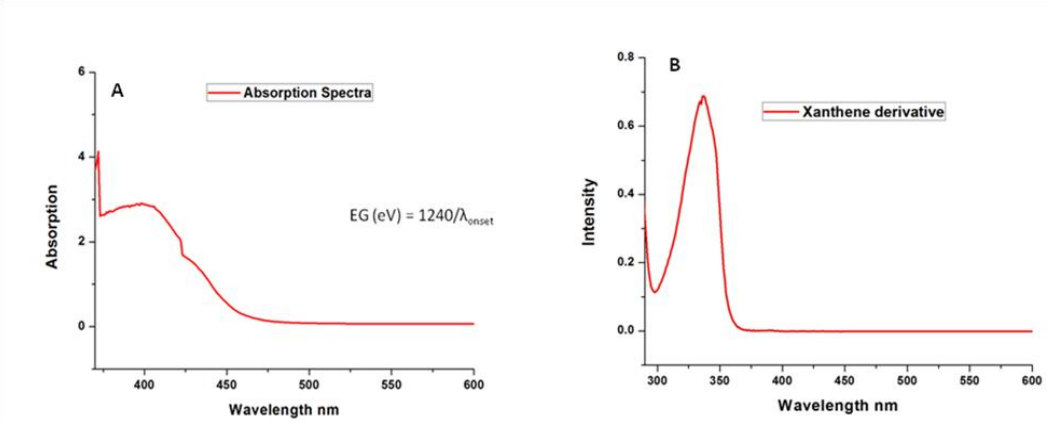


**Figure 3**. UV – Vis Spectra. A) Absorption maxima of flourene derivative in methanol is 400 nm which is attributed to the $\pi$-$\pi^*$ transition with energy gap of 3.1eV. Flourenyl is rigid and bulky. B) Absorption maxima of xanthene derivative in ethanol is 337 nm which is attributed to the $\pi$-$\pi^*$ transition with energy gap of 3.6 eV.

*3.4. Flourescence spectroscopy*

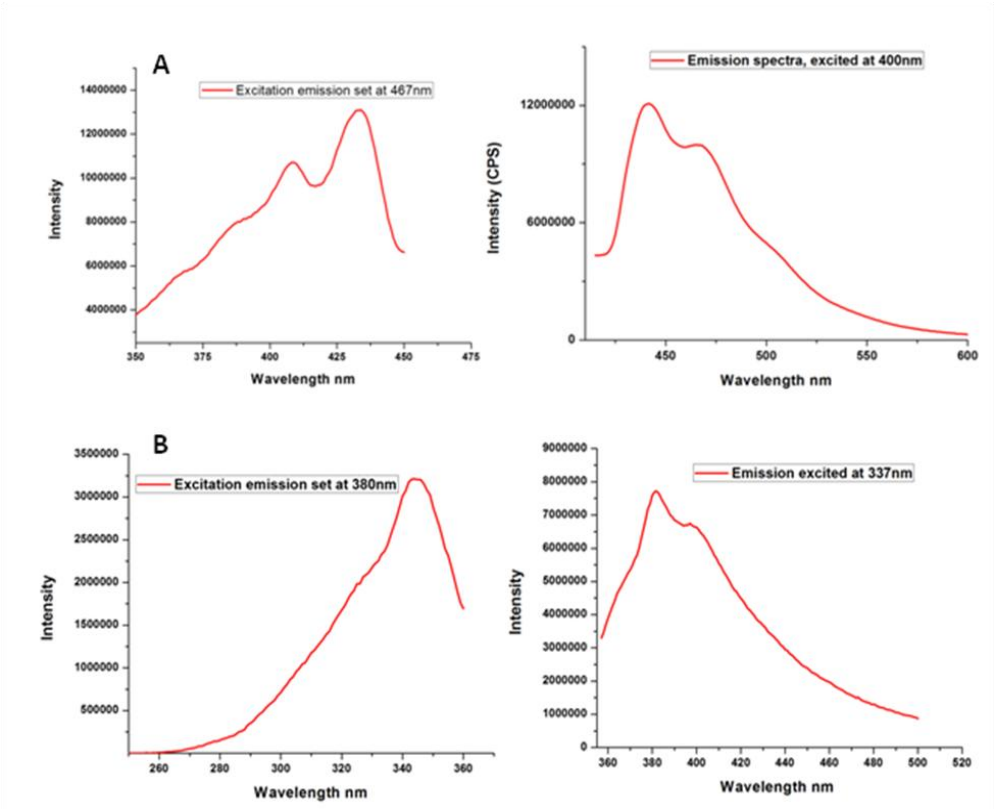


**Figure 4.** A) Emission and excitation spectra for flourene derivative. B) Emission and excitation spectra for xanthene derivative.

Fig 4A reveals the excitation and emission spectra of flourene derivative with excitation maxima of 433 and emission maxima of 441 nm. It also reveals a vibronic structure which is correlated with a coupled C=C stretching mode (1603-1447 $cm^{-1}$) and small stokes shift of 8nm [16]. Well-defined vibronic structure specifies a rigid and well-defined backbone [9]. Small stokes shift is a result of J-aggregates whereby molecular arrangement in which the transition moment of individual monomers are aligned parallel to the line joining their centers. A similar spectra has been observed for poly[(1,4-phenylene)-2,7-(9,9-dioctylfluorene)] [9]. Fig 4B shows excitation and emission spectra of xanthene derivative. The maximum emission band is located at 380 nm and the excitation maxima is 344 nm with a stoke shift of 36 nm.

### *3.5. Powder x-ray diffraction (PXRD)*

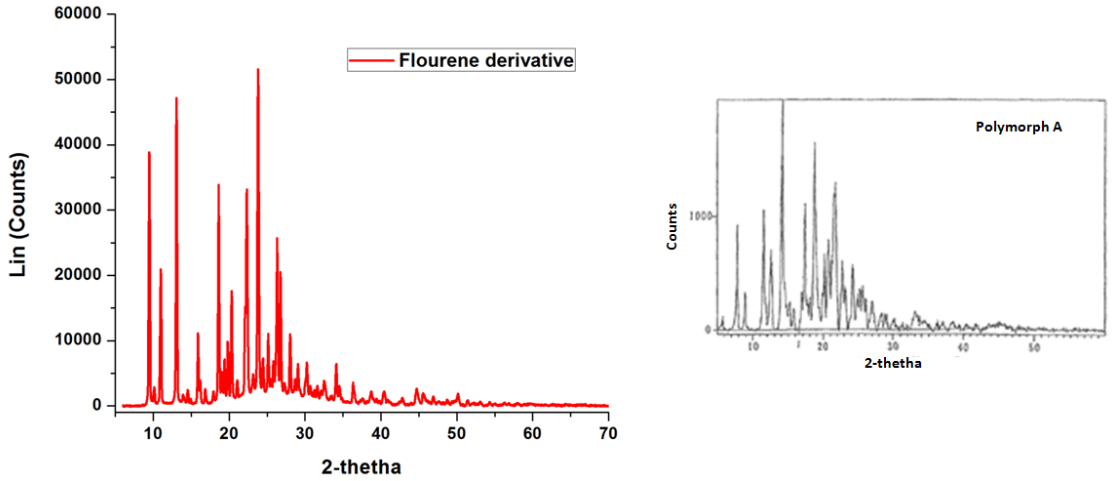


**Figure 5(a).** Powder pattern for 9,9'-(ethyne-1,2-diyl)bis(flouren-9-ol) (red) and 9,9-bis(4-(2-hydroxyethoxy) phenyl) fluorene (black).

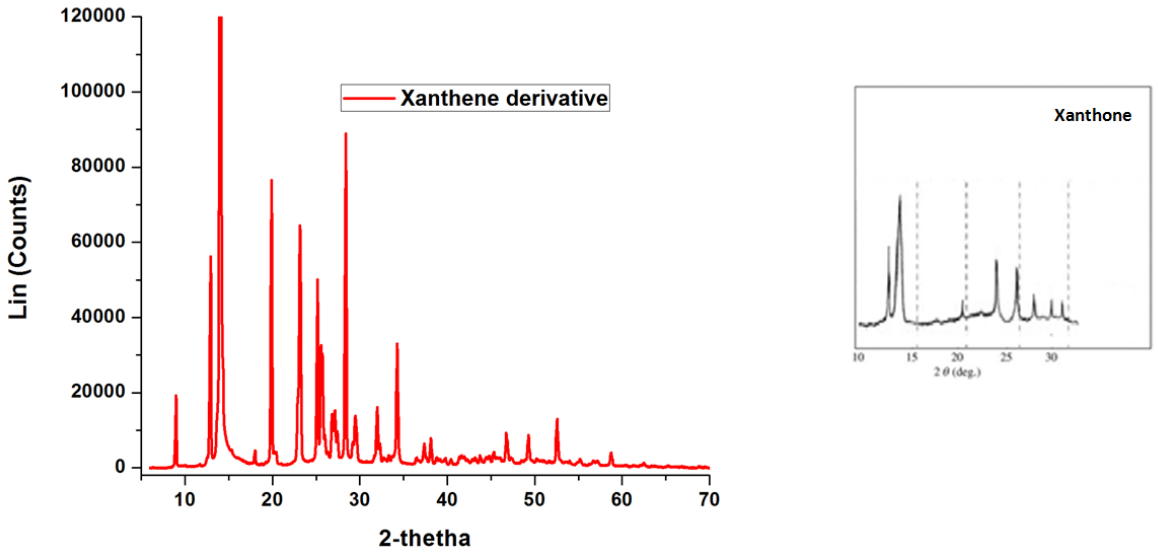


**Figure 5(b).** Xanthene derivative powder pattern (red) and xanthone powder pattern (black).

PXRD was used to observe the phase changes (size, shape and symmetry of the unit cell). Fig 5A shows a powder pattern for 9,9'-(ethyne-1,2-diyl)bis(flouren-9-ol) referred to as flourene derivative. Similar powder pattern were observed for 9,9-bis(4-(2-hydroxyethoxy) phenyl) fluorene and 9,9-bis(4-hydroxyphenyl) fluorene [17].

Fig 5B reveals a powder pattern for xanthene derivative which is different from that of the starting material xanthone [18]. This confirms that 9-(4-methoxyphenyl)-9H-xanthen-9-ol was indeed synthesized. Both powders flourene derivative and xanthene derivative had shown an orthorombic shape with a volume of 3750.55 $Å^3$ for flourene derivative and volume of 954.25 $Å^3$ for xanthene derivative.

### *3.6. Cyclic voltammetry (CV) and Square wave voltammetry (SWV)*

Electrochemistry of flourene derivative and xanthene derivate was investigated using CV and SWV. Fig 6A&B shows a typical cyclic voltammogram of flourene derivative and xanthene derivative respectively. Reversible oxidation-reduction peaks were observed with peak separation of 75.4 mV for one electron redox which means that the system is quasi reversible (flourene derivative) and peak separation of 59.95 mV for one electron redox which means that the system is fully reversible (xanthene derivative). Peak separation of 80 mV for the reversible wave of flourene derivative FDF was observed [19]. For both flourene derivative and xanthene derivative the peak current magnitude was observed to increase upon increment of the scan rate signifying the peak currents are diffusion controlled. Diffusion coefficient and surface concentration were calculated from plots of current versus square root of scan rate from CV data and based on the slope of peak current versus dimensionless peak current plot from SWV data (fig 7A&B) using the Randle Sevcik equation:

$$I_p = 2.69 \times 10^5 n^{3/2} A D^{1/2} v^{1/2} C$$

where $I_p$ = peak current, n = number of electron transfer, A = area of an electrode, D = diffussion coefficient, v = scan rate and C = concentration of bulk solution[20]. The results for both CV and SWV are tabulated in table 1 below.

**Table 1.** Calculated parameters from electrochemical techniques (CV and SWV).

| **Product** | **$D_e$** | | **Formal Potential** | **Surface concentation** |
|---|---|---|---|---|
| | **CV** | **SWV** | | |
| **Flourene derivative** | $8.91 \times 10^{-6} cm^2 s^{-1}$ | $1.78 \times 10^{-16} cm^2 s^{-1}$ | -134 mV | $1.55 \times 10^{-13}$ molcm$^{-2}$ |
| **Xanthene derivative** | $1.05 \times 10^{-10} cm^2 s^{-1}$ | $4.02 \times 10^{-16} cm^2 s^{-1}$ | -73.5 mV | $2.00 \times 10^{-13}$ molcm$^{-2}$ |

Surface concentration for both compounds was found to be smaller when compared to PANI films which gave the surface concentration of the order of $10^{-8}$ molcm$^{-2}$ [21] and ferrocenyl disulfides had shown to have surface concentration of the order of $10^{-10}$ molcm$^{-2}$. These are regarded as self-assembly monolayer [22]. Scan rate dependent cyclic voltammetry (CV) confirmed the

electrodynamics of the thin films to be consistent with monolayer diffusion for both compounds. The theoretical value for diffusion coeffient by Kaifer et. al based on cyclodextrin derivatives was found to have the same magnitude as the one we obtained for flourene derivative ($10^{-6}$ $cm^2s^{-1}$) [23].

Xanthene derivative is in good agreement with the diffusion coefficient calculated for polymer (G1 PPI) poly(propylene imine) ($10^{-10}$ $cm^2s^{-1}$) [24]. This place our values obtained for the diffusion coefficient well within the range of modified surfaces employing clathrates and polymers. The values for De obtained from SWV were much lower and showed no correlation with the values obtained from CV data, since the SWV calculation is based on extracted values for dimensionless currents.

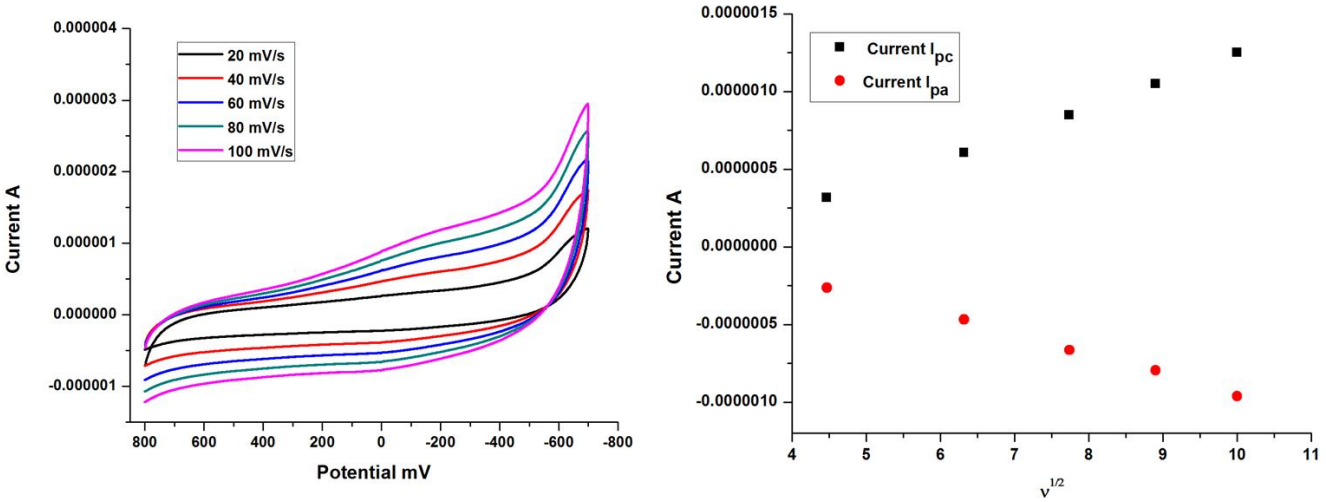


**Figure 6(a).** Cyclic voltammograms flourene derivative on GCE in 0.2 M PBS pH 7.12. Scanrate ($\nu^{1/2}$). Plot of $i_{pc}$ /$i_{pa}$ versus scanrate$^{1/2}$ from voltammograms.

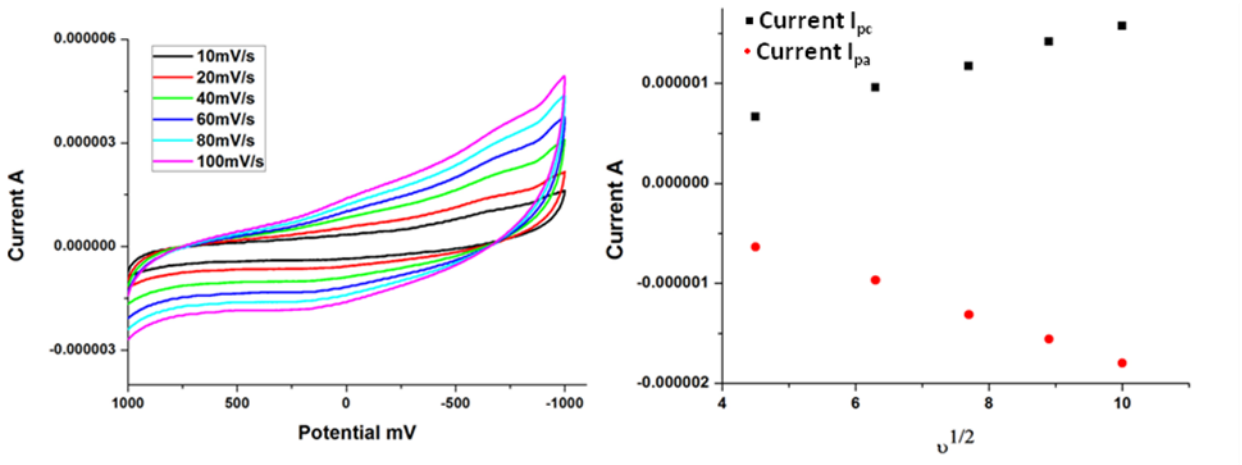


**Figure 6(b).** Cyclic voltammograms of xanthene derivative on GCE in 0.2 M PBS pH 7.12. Scanrate ($\nu^{1/2}$). Plot of $i_{pc}$ /$i_{pa}$ versus scanrate$^{1/2}$ from voltammograms.

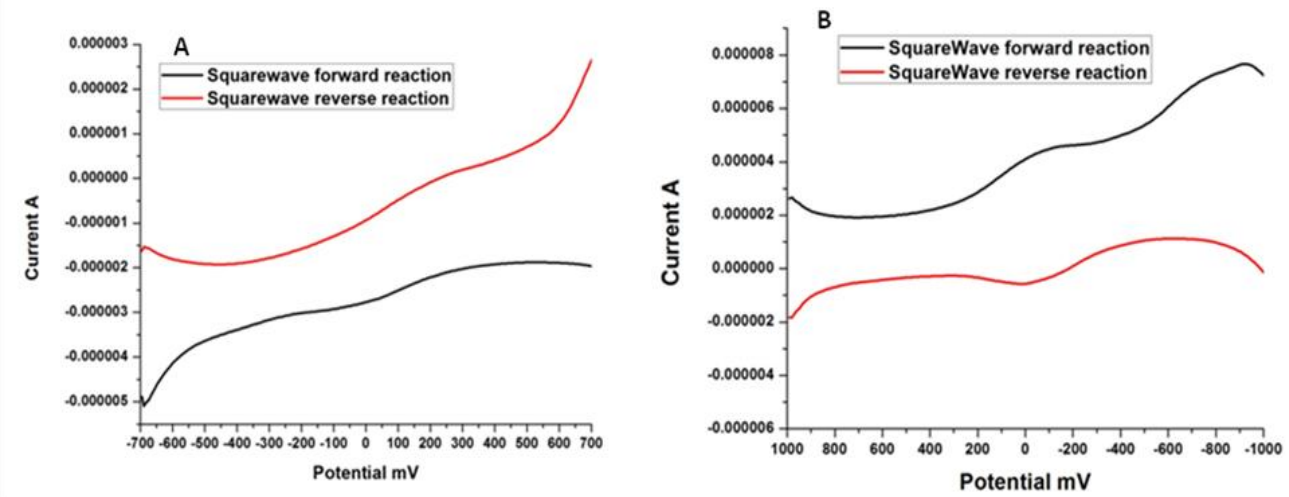


**Figure 7.** A) Flourene derivative SWV data with the formal potential of -134 mV. B) Xanthene derivative SWV data with the formal potential of -73 mV.

*3.7. Electrochemical impedance spectroscopy (EIS)*

The impedance data was modelled as a simple Randles circuit with a single RC loop. The parameter resulting from circuit fitting study are listed in table 2 such as solution resistance $R_s$, double layer capacitance $C_{dl}$ and charge transfer resistance $R_{ct}$. These parameters were used to calculate the time constant ($\tau$) using equation 2, the exchange current ($i_0$) using equation 3 and homogeneous rate constant using equation 4[25]. The results are listed in table 2.

**Table 2.** EIS parameters obtained from the circuit fitting of impedance data for GCE/F and GCE/X and calculated results for time constant, exchange current and homogeneous rate constant for GCE/F and GCE/X.

| Parameter | GCE/F | GCE/X |
|---|---|---|
| Electrolyte resistance ($R_s$) Ohms | 12.56 | 206.2 |
| Charge transfer resistance ($R_{ct}$) Ohms | $9.128 \times 10^{6}$ | $4.40 \times 10^{6}$ |
| Double layer capacity ($C_{dl}$) µF | 35.45 | 26.9 |
| Time constant ($\tau$) s $rad^{-1}$ | 3.24 | 1.18 |
| Exchange current ($i_o$) A | $1.41 \times 10^{-9}$ | $2.92 \times 10^{-9}$ |
| Homogeneous rate constant ($K_{et}$) $cms^{-1}$ | $1.03 \times 10^{-12}$ | $2.13 \times 10^{-12}$ |

$$\tau = R_{ct} C_{dl} \qquad \text{Equation (2)}$$

$$i_0 = \frac{RT}{nFR_{ct}} \qquad \text{Equation (3)}$$

$$i_0 = nFAK_{et}C^* \qquad \text{Equation (4)}$$

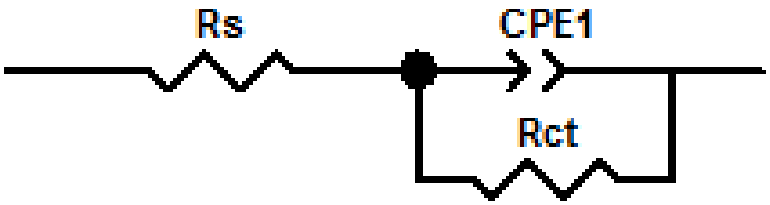


**Figure 8.** Equivalent circuit used for all impedance analysis.

Solution resistance **Rs** is the resistance between the working electrode and the reference electrode. This is shown by a small offset on the real impedance axis. It is measured at high frequency intercept near the origin of the nyquist plot. Charge transfer resistance **Rct** is the resistance associated with the charge transfer mechanism for the electrode reactions. It is the resistance to electron transfer at the electrode interface. Constant phase element **CPE** is a non-intuitive circuit element that was invented while looking at the response of real-world system. Normally it is used in a model in place of a capacitor due to deviation of capacitance parameters from expected values (inhomogenities at the interface)[25].

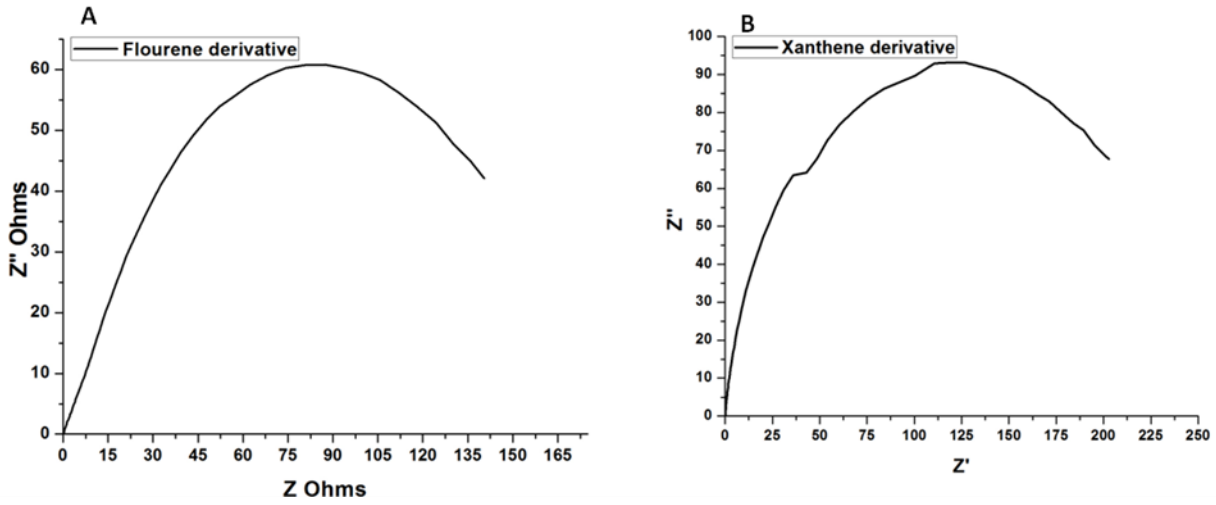


**Figure 9.** Nyquist diagram. A = Flourene derivative. B = Xanthene derivative.

## 4. CONCLUSION

Yellow solution was observed for both clathrate compounds. For both derivatives, it was concluded that they are semiconductors due to their energy gap 3.1 eV for flourene and 3.6 eV for xanthene derivative. Reversible oxidation-reduction peaks were observed for both clathrates compounds with similar diffusion coeffient ($D_e$) from both CV and SWV data. $D_e$ was found to be $8.91x10^{-6}cm^2s^{-1}$from CV data and $1.78x10^{-16}$ from SWV data and $1.05x10^{-10}cm^2s^{-1}$ from CV data and

$4.02x10^{-16}$ $cm^2s^{-1}$ from SWV data and these values are within the range of modified surfaces employing polymers. From EIS data capacitance was found to be 35.45 μF for xanthene derivative and 26.9 μF for xanthene derivative. Both clathrates compounds behaved in almost same manner.

FTIR and PXRD confirmed both clathrate structures. Previously porous macrocyclic compounds with cavity have been used whereby the guest molecule is temporarily locked or caged within the host cavities. Gold nanoparticles have been used in the immunosensor development for these macrocyclic compounds, they act as tiny conducting centres facilitating normal electron transfer kinetics. Small stokes shift have been observed from the flourescence which confirmed that these compounds are rigid and have a well-defined backbone. Both compounds are electroactive confirmed by SWV, CV and EIS. For future work Flourene derivative and xanthene derivative will be utilized in the immunosensor deveopment whereby a conductive transducer (gassy carbon electrode) will be used. The antibody will be immobilized directly onto these clathrates compounds.

ACKNOWLEDGEMENTS
We gratefully acknowledge financial support from National Research Foundation (NRF) South Africa and University of the Western Cape (UWC).

**References**

1. E. Weber, S. Nitsche, A. Wierig, I. Csöregh, *Eur. J. Org. Chem.,* (2002) 856-872.
2. P. He, J. Ye, Y. Fang, I. Suzuki, T. Osa, *Anal. Chim. Acta.,* 337 (1997) 217-223.
3. C. Retna Raj, R. Ramaraj, *Electrochim. Acta.,* 44 (1999) 2685-2691.
4. G.G. Surpateanu, M. Becuwe, N.C. Lungu, P.I. Dron, S. Fourmentin, D. Landy, G. Surpateanu, *J. Photochem. Photobiol. A: Chem.,* 185 (2007) 312-320.
5. K.M. Molapo, P.M. Ndangili, R.F. Ajayi, G. Mbambisa, S.M. Mailu, N. Njomo, M. Masikini, P. Baker, E.I. Iwuoha, *Int. J. Electrochem. Sci.,* 7 (2012).
6. W.S. Matthews, J.E. Bares, J.E. Bartmess, F. Bordwell, F.J. Cornforth, G.E. Drucker, Z. Margolin, R.J. McCallum, G.J. McCollum, N.R. Vanier, *J. Amer. Chem. Soc.,* 97 (1975) 7006-7014.
7. T. Arumanayagam, P. Murugakoothan, *J. Miner. Mater. Character. Eng.,* 10 (2011) 1225-1231.
8. K.-T. Wong, Y.-M. Chen, Y.-T. Lin, H.-C. Su, C.-c. Wu, *Org. lett.,* 7 (2005) 5361-5364.
9. M. Ranger, D. Rondeau, M. Leclerc, *Macromol.,* 30 (1997) 7686-7691.
10. V. Martínez Martínez, F. López Arbeloa, J. Bañuelos Prieto, T. Arbeloa López, I. López Arbeloa, *J. Phys. Chem. B.,* 108 (2004) 20030-20037.
11. C. Tang, F. Liu, Y.-J. Xia, J. Lin, L.-H. Xie, G.-Y. Zhong, Q.-L. Fan, W. Huang, *Org. electron.,* 7 (2006) 155-162.
12. P.-I. Shih, C.-L. Chiang, A.K. Dixit, C.-K. Chen, M.-C. Yuan, R.-Y. Lee, C.-T. Chen, E.W.-G. Diau, C.-F. Shu, *Org. lett.* 8 (2006) 2799-2802.
13. Y. Wei, W.W. Focke, G.E. Wnek, A. Ray, A.G. MacDiarmid, *J. Phys. Chem.,* 93 (1989) 495-499.
14. H.S. Abdulla, A.I. Abbo, *Int. J. Electrochem. Sci.,* 7 (2012) 10666-10678.
15. O. Tovide, N. Jaheed, N. Mohamed, E. Nxusani, C.E. Sunday, A. Tsegaye, R.F. Ajayi, N. Njomo, H. Makelane, M. Bilibana, *Electrochim. Acta.,* 128 (2014) 138-148.
16. K.D. Belfield, M.V. Bondar, O.V. Przhonska, K.J. Schafer, W. Mourad, *J. Lumin* 97 (2002) 141-146.
17. K. Fujii, K. Fukui, *Google Patents.*, 2012.
18. T. Shimo, M. Matsushita, H.I. Omar, K. Somekawa, *Tetrahedron* 61 (2005) 8059-8064.

19. K.M. Omer, S.Y. Ku, K.T. Wong, A.J. Bard, *Angew. Chem. Inter. Ed.*, 48 (2009) 9300-9303.
20. R.A. Olowu, O. Arotiba, S.N. Mailu, T.T. Waryo, P. Baker, E. Iwuoha, *Sensors.*, 10 (2010) 9872-9890.
21. M. Muchindu, T. Waryo, O. Arotiba, E. Kazimierska, A. Morrin, A.J. Killard, M.R. Smyth, N. Jahed, B. Kgarebe, P.G. Baker, *Electrochim. Acta.*, 55 (2010) 4274-4280.
22. R.C. Sabapathy, S. Bhattacharyya, M.C. Leavy, W.E. Cleland, C.L. Hussey, *Langmuir.*, 14 (1998) 124-136.
23. C.M. Cardona, T.D. McCarley, A.E. Kaifer, *J. Org. Chem.*, 65 (2000) 1857-1864.
24. O.A. Arotiba, J.H. Owino, P.G. Baker, E.I. Iwuoha, *J. Electroanal. Chem.*, 638 (2010) 287-292.
25. A.J. Bard, L.R. Faulkner, *Wiley New York*, 1980.